RSC Advances

PAPER

View Article Online
View Journal | View Issue



Cite this: *RSC Adv.*, 2020, **10**, 3493

# Biomethane generation from biogas upgrading by means of thin-film composite membrane comprising Linde T and fluorinated polyimide: optimization of fabrication parameters

Norwahyu Jusoh, *[ab] Yin Fong Yeong,[b] Serene Sow Mun Lock,[bc] Li Sze Lai[d] and Malik Shoaib Suleman[e]

Generation of biogas from organic substances is an attractive evolution of energy generation from fossil-based energy supply to renewable resources. In order to exhibit viability in terms of technical execution while being economically feasible, successful purification strategies for biomethane formation must be applicable to industrial gas streams at realistic pressures and temperatures. Membrane-based upgrading technologies have great potential to promote biogas processes because they involve less energy and low maintenance. However, the development of membranes with good polymer-filler contact and minimum defects remains a great challenge. Hitherto, researchers have been making many attempts at developing an established route to fabricate thin-film composite membranes. In the present work, an innovative coupling between Linde T and fluorinated polyimide was employed for biogas upgrading. A facile technique for membrane fabrication was proposed *via* optimization of the fabrication parameters. The results indicated that composite membrane fabricated with 2 hours of total dispersion duration demonstrated a homogeneous distribution of Linde T particles in the fluorinated polyimide matrix and improved the separation characteristics by up to 172% in upgrading biomethane quality. Thus, the fabricated membrane is feasible to be employed for large-scale and lucrative production with enhanced performance in biogas purification *via* the feasible fabrication method employed in this work.

Received 14th August 2019
Accepted 22nd December 2019

DOI: 10.1039/c9ra06358g

rsc.li/rsc-advances



## 1 Introduction

The current alarming phenomenon in the shortage of the global energy market has diverted attention towards increasing the production of renewable energy from geothermal, wind, waste, biomass and solar sources in order to meet the needs of global energy consumption.[1] As a result of the soaring costs of conventional fuels, anaerobic digestion of biological resources is identified as a promising alternative energy carrier as it is clean, environmentally benign and cheap.[2] Biogas generated *via* anaerobic digestion normally consists of 50–70% of $CH_4$, 25–50% of $CO_2$ and other gases including $N_2$, $H_2S$, siloxane and halides.[3] Efficiency of current biogas production processes is restricted due to gas streams being produced with dilute content of $CH_4$. Thus, biogas enrichment is a critical downstream stage which accounts for the overall production success. The biogas upgrading process comprises the removal of $CO_2$ and other impurities to afford biomethane with higher $CH_4$ concentration and heating value that can be subsequently utilized for combined heat and power engines and natural gas substitution.[4]

In industrial practice, biogas purification can be accomplished using available technologies including adsorption, cryogenic, absorption and membrane separations. The shortcomings of large footprint, high cost consumption, solvent flow problems and high energy required by absorption, adsorption and cryogenic processes have provoked interest in membrane technology as an alternative means of recovery of biomethane.[5] The first establishment of membranes for biogas enrichment plant was commercialized in 1990 and the application of membranes in upgrading biogas has led to more researchers to explore membrane materials with advanced gas transport properties for the purification process, which ultimately favors environmental and energy-related processes as an end result.[6]

[a]*Centre for Contaminant Control & Utilization (CenCoU), Chemical Engineering Department, Universiti Teknologi PETRONAS, 32610 Bandar Seri Iskandar, Perak, Malaysia. E-mail: norwahyu.jusoh@utp.edu.my; Fax: +605-3656176; Tel: +605-3687614*

[b]*$CO_2$ Research Centre ($CO_2$RES), Chemical Engineering Department, Universiti Teknologi PETRONAS, 32610 Bandar Seri Iskandar, Perak, Malaysia*

[c]*Chemical Engineering Discipline, School of Engineering, Monash University Malaysia, Jalan Lagoon Selatan, 47500 Bandar Sunway, Selangor, Malaysia*

[d]*Chemical and Petroleum Engineering Department, Faculty of Engineering, Technology and Built Environment, UCSI University Kuala Lumpur Campus, Jalan Mandarina Damai 1, 56000 Bandar Cheras, Kuala Lumpur, Malaysia*

[e]*Department of Chemical Engineering, Sharif College of Engineering & Technology, Jati Umrah, Raiwind Road, Lahore, Pakistan*

For biogas upgrading processes, membrane materials that demonstrate good mechanical strength as well as superior gas permeability and gas pair selectivity are anticipated. Membranes are commonly prepared through a combination of polymeric materials, *e.g.* polysulfone, cellulose triacetate, and polycarbonate, and inorganic materials such as silica, zeolite, carbon molecular sieves and metal organic frameworks.[7] Despite the advantage that a polymeric membrane is easy to form that has a cost benefit, this material suffers from a universal trade-off relationship between gas permeability and selectivity as discovered by Robeson.[8] In addition, inorganic membranes have also been examined for gas separation due to their promising characteristics such as high permeability and selectivity, and good thermal and chemical stability. Nevertheless, inorganic membranes are expensive and complicated to fabricate and scale up in comparison to polymeric membranes.[9] Hence, researches have been devoted to fabrication of membrane materials which could preserve the good traits of both polymeric and inorganic membranes.

Composite membranes have been developed by incorporating dispersed fillers into the polymer phase to overcome the aforementioned drawbacks and also to enhance separation performances of the membranes which can be subsequently employed for industrial applications including biogas cleaning.[10,11] The selections of polymer and filler are crucial to ensure a good polymer-filler compatibility which can subsequently improve gas separation performance of the resultant composite membranes in biogas purification. The utilization of polyimides as a continuous phase in the fabrication of composite membranes has been increasing steadily owing to their excellent physicochemical and mechanical behaviors.[12] Present trends show that fluorinated polyimide is an attractive material for fabrication into composite membranes because of its remarkable separation performance including high chemical, mechanical and thermal stability and solvent resistance attributes.[13] The presence of bulky methyl groups and $-C(CF_3)_2-$ in the backbone of the polymer hinders local segmental mobility and impedes interchain packing, which result in the enhancement of separation performance through bigger free channels for gas transport.[14,15]

Zeolites are inorganic fillers, which have been widely studied by researchers for biogas purification processes.[7,16–18] Zeolites are porous crystalline compounds, containing elements of Al and Si with cations like Ca, K, Na and Mg, which are arranged in a tetrahedral structure. The properties of zeolites, such as uniform charge distribution, well-defined pore size, high porosity and high specific area, make them appealing candidates for the removal of $CO_2$ from raw biogas.[19,20] A-type zeolites, Faujasite (zeolite X and Y), Zeolite Socony Mobil-5 (ZSM-5), and SAPO-34 are types of zeolites which have been widely used in the fabrication of composite membranes for biogas purification. For instance, Sen *et al.*[21] reported the enhancement of $CO_2/CH_4$ selectivity from 23.6 to 37.6 by embedding 30% of zeolite 4A into a polycarbonate polymer phase. Furthermore, Amooghin *et al.*[22] found that by embedding 5% of zeolite Y in a Matrimid®5218 membrane, both $CO_2$ permeability and $CO_2/CH_4$ selectivity were enhanced in comparison to the pristine membrane. Furthermore, the amalgamation of SAPO-34 into a polysulfone matrix has been reported by Junaidi *et al.*[23] They discovered that a membrane composed of 5 wt% SAPO-34 particles significantly improved selectivity in removing $CO_2$ from raw biogas of up to 30% relative to a pure polysulfone membrane.

Even though the separation performances of zeolite-based composite membranes were improved, most of the reported performances are still unable to meet expectation with regards to tradeoff between permeability and selectivity.[24–26] Hence, to address these bottlenecks, it is crucial to explore a new combination of zeolite and polymer matrix. Linde T has been identified as one of the potential materials for biogas upgrading due to its desirable traits including great tolerance towards acids and solvents, good thermal stability, and ability to interact with adsorbates at low pressure or concentration.[27] In addition, the presence of heterogeneous cations in Linde T offers a stronger interaction for $CO_2$ because it exhibits higher quadrupole moment and polarizability as compared to biomethane, which consequently leads to a higher affinity for the $CO_2$ adsorption process.[28] Moreover, the Linde T structure is made up of 8-membered oxygen rings, which contribute to a small pore size of 0.36 nm $\times$ 0.51 nm, further contributing to greater separation of gases including $CO_2$ from biomethane.[29] For example, Mirfendereski *et al.*[30] reported a selectivity for a Linde T membrane of up to 70.8 in removing $CO_2$ from $CH_4$. Hence, the promising reported separation performance for Linde T has motivated the present work to further elucidate the potential of Linde T as an inorganic filler in the fabrication of composite membranes for capturing $CO_2$ from raw biogas.

In addition, although enhancement of gas separation performance has been reported *via* application of zeolite-based composite membranes, the distribution of fillers in the polymer phase remains a severe challenge in producing membranes, requiring further understanding of the fabrication parameters. Indeed, most of the researches reported on composite membranes have been dedicated to merely studying the enhancement of permeability and selectivity of the membranes,[31–33] whereas studies on finding an appropriate approach for the formation of zeolite-based composite membranes *via* optimization of the fabrication parameters have been scarce. A thorough attempt at examining the fabrication variables in detail can have a substantial influence on the formation of membranes. This is because fabrication of composite membranes with excellent quality involves stringent settings during processing, meaning that the approaches to fabricate composite membranes are relatively tiresome, tedious, and normally not economically viable. Thus, these challenges need to be overcome in order to obtain the preferred membrane characteristics of high reproducibility and to improve gas separation properties for biogas upgrading processes.

Hence, elucidation of the basic parameters, which include dispersion duration of filler in solvent and polymer solution during fabrication of composite membranes, is discussed in the present work. The physicochemical properties of the resulting composite membranes were analyzed using various analytical tools. Furthermore, permeation properties of the resultant

 

membranes in upgrading biomethane were also examined. To the best of our knowledge, studies on the combination of Linde T and fluorinated polyimide polymer for biogas upgrading are yet to be reported.

## 2 Experimental method

### 2.1 Materials

Synthesis of Linde T required potassium hydroxide (KOH, 85 wt%, Merck), precipitated silica ($SiO_2$, 99.8 wt%, Aldrich), sodium hydroxide (NaOH, 99 wt%, Merck), deionized water and sodium aluminate ($NaAlO_2$, BDH [$Na_2O$, 41 wt% + $Al_2O_3$, 54 wt%], Aldrich). All these chemicals were utilized without further purification. Meanwhile, for the preparation of fluorinated polymer, 4,4′-(hexafluoroisopropylidene)diphthalic anhydride (99% purity, Sigma-Aldrich), *N*-methyl-2-pyrrolidone (NMP) and 2,3,5,6-tetramethyl-*p*-phenylenediamine (99% trace metal basis, Sigma-Aldrich) were refined by vacuum sublimation, vacuum distillation and re-crystallization from methanol, respectively. Triethylamine (TEA, ≥99% purity, Merck), propionic anhydride (PA, ≥98% purity, Merck), dichloromethane (DCM, ≥99.8% purity, Sigma-Aldrich) solvent and methanol (≥99.9% purity, Merck) were used as received. All pure gases including methane ($CH_4$, 99.99%) and carbon dioxide ($CO_2$, 99.99%) as well as gas mixtures ($CO_2$ 50 vol% + $CH_4$ 50 vol%) for permeation experiments were acquired from Gas Walker Sdn Bhd and utilized as received.

### 2.2 Synthesis of fluorinated polyimide

Fluorinated polyimide was synthesized using the chemical imidization method.[34] Equimolar purified monomers were dissolved in refined NMP under nitrogen purge after stirring for 24 h to form polyamic acid (PAA) solution. For the chemical imidization process, TEA and PA with a molar ratio of 1 : 4 were added slowly into the PAA solution. Then, the solution was further stirred for 24 h to form a polymer solution. The resultant polymer solution was suspended in methanol in order to remove unreacted monomers. The polymer was then washed with methanol prior to drying at 150 °C in a vacuum oven for 24 h. The reaction scheme for synthesizing fluorinated polyimide polymer and the chemical structure of the resultant polymer are shown in Fig. 1.[35] The inherent viscosity and number-average molecular weight ($M_n$) of the synthesized fluorinated polymer were 0.64 dL $g^{-1}$ and 59 000 g $mol^{-1}$, respectively, which is in good agreement with the reported results in previously published literature.[36]

### 2.3 Preparation of Linde T crystals

Linde T crystals were synthesized using a gel of $SiO_2 : 0.04Al_2O_3 : 0.26Na_2O : 0.09K_2O : 14H_2O$ composition *via* hydrothermal growth coupled with ultrasonic irradiation. Firstly, deionized water was utilized to dissolve sodium hydroxide and potassium hydroxide. Later on, sodium aluminate was added into the solution before being stirred for 1 h. Precipitated silica was subsequently added into the solution progressively while being stirred for another 24 h. After that, ultrasonic treatment at a frequency of 40 kHz (SOLTEC, Model 2400 EP) was utilized to pretreat the solution for 1 h, prior to transferring the solution into a Teflon-lined stainless steel autoclave reactor. Inside the reactor, the solution was treated at 120 °C for 1 day to achieve hydrothermal growth. Finally, solid particles were collected through centrifugation and washed using deionized water prior to drying at 120 °C in an oven.

### 2.4 Preparation of virgin fluorinated polyimide membrane

Virgin fluorinated polyimide flat sheet membrane was fabricated by preparing a 2% (w/v) polymer solution using the solution casting method.[37] Initially, the synthesized polymer was dissolved in DCM and left stirring which was completed within 1 h. Then, the mixture was filtered using a 1.0 μm PTFE membrane filter to eliminate any undesirable contaminants and debris. The solution was then cast in a Petri dish and covered with a glass plate to induce slow solvent evaporation. The membrane was dried in a conventional oven at 60 °C for 24 h prior to vacuum drying. In the vacuum oven, a drying protocol involving increasing the temperature to 250 °C utilizing a heating rate of 25°C $h^{-1}$ was carried out, followed by annealing at 250 °C for 24 h.

### 2.5 Fabrication of Linde T/fluorinated polyimide composite membranes

A composite membrane with 1 wt% Linde T in fluorinated polyimide phase was used as a benchmark for the study on the manipulation of dispersion duration of Linde T in DCM suspension under different stirring and sonication periods. The total filler dispersion duration was varied from 2 h to 8 h. Firstly, solutions of both fluorinated polyimide and Linde T were formulated in two separate vials. 1 wt% of Linde T crystals were added into DCM, stirred and sonicated successively for 1–4 h to disperse Linde T in DCM solution. In order to ensure consistency in the experimental works, the stirring process was conducted using a WiseStir MSH-20D magnetic stirrer with a 1.8 cm in length and 0.4 cm in diameter stirring bar, whereas sonication was conducted in an ultrasonication water bath operated at 40 kHz and 120 W throughout the experiments. Meanwhile, fluorinated polyimide was dissolved in DCM and the solution was filtered to eliminate any insoluble particles and undesirable impurities. Then, 10 wt% of fluorinated polyimide solution was primed into Linde T particle solution before stirring and sonification treatment. Subsequently, the stirring and sonification procedure was further continued for another 1–4 h after addition of the remaining bulk polyimide solution into the mixture. The mixture was then vigorously stirred before pouring the casting solution into a leveled and clean glass Petri dish. The speed of stirring and vigorous stirring for the preparation of all solutions were maintained consistent throughout the experiment. The formed membrane film was peeled off from the Petri dish with care before being sent for heat treatment, which has been elaborated in Section 2.4 describing the preparation of virgin fluorinated polyimide membrane. The composite membranes that were obtained by means of manipulation of fabrication parameters are summarized in Table 1.

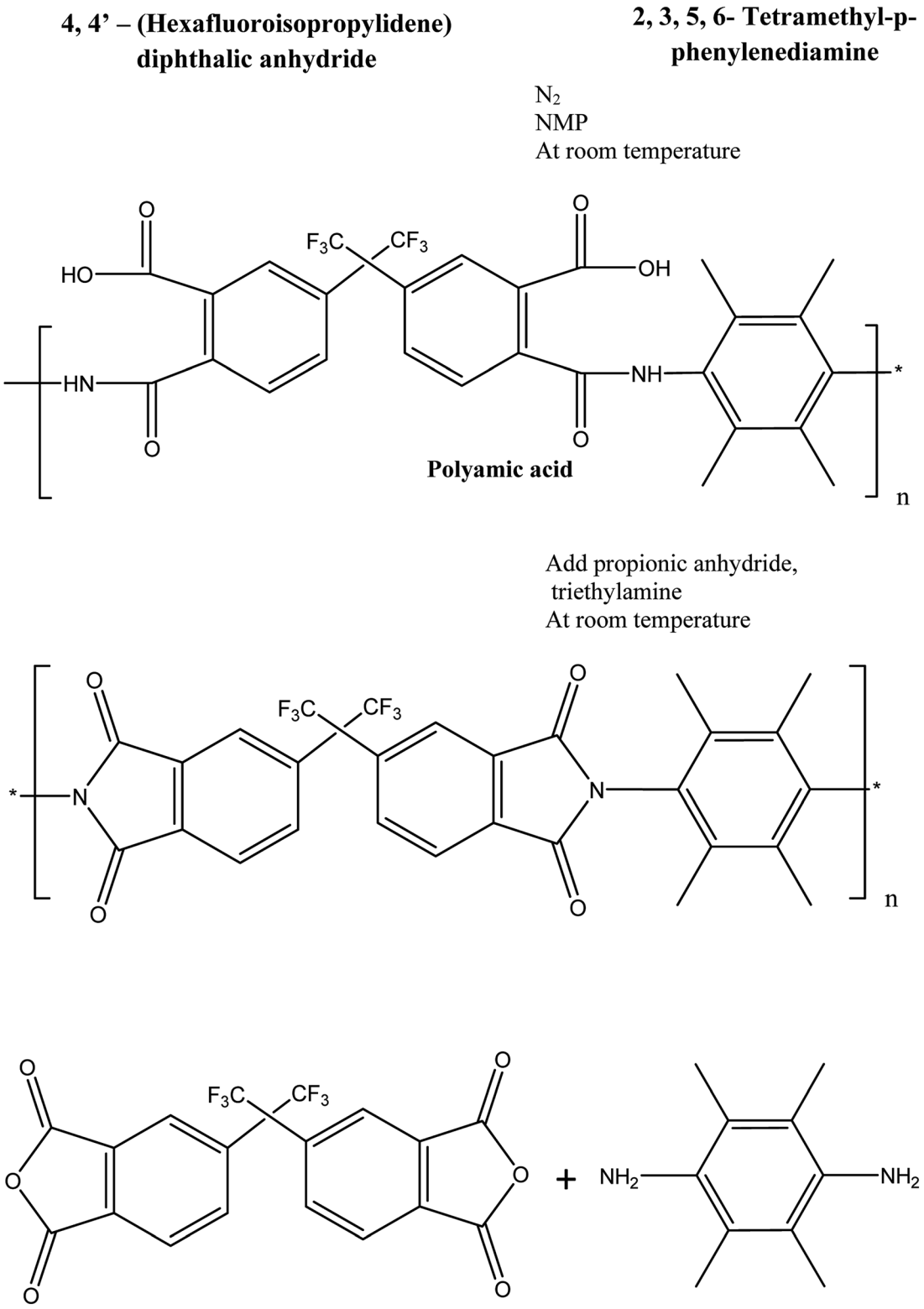


Fig. 1 Schematic showing the formation of fluorinated polymer.[35]

### 2.6 Characterization of fluorinated polyimide polymer, Linde T particles and membranes

The molecular weight of the synthesized fluorinated polyimide polymer was determined using gel permeation chromatography (GPC). A Waters HPLC 1500 series system equipped with a 2414 refractive index detector and Styragel HR columns was employed to perform GPC measurements. Tetrahydrofuran with a flow rate controlled at 1.0 mL $min^{-1}$ was utilized as the

 

Table 1 Linde T/fluorinated polyimide composite membranes fabricated in the current work by using different durations of filler dispersion

| | Filler dispersion duration | | | | |
|---|---|---|---|---|---|
| | Linde T in DCM | | Linde T in fluorinated polyimide solution | | |
| Membrane sample | Stirring (h) | Sonication (h) | Stirring (h) | Sonication (h) | Total dispersion duration (h) |
| S1 | 0.5 | 0.5 | 0.5 | 0.5 | 2 |
| S2 | 1 | 1 | 1 | 1 | 4 |
| S3 | 1 | 1 | 2 | 2 | 6 |
| S4 | 2 | 2 | 1 | 1 | 6 |
| S5 | 2 | 2 | 2 | 2 | 8 |

solvent. A standard polystyrene sample of 0.004 wt% was used to calibrate the column. The value obtained for standard polystyrene was employed as a benchmark to determine molecular weights (g $mol^{-1}$) of other solutions through comparison of retention time within the column *via* a calibration curve. In addition, an Ubbelohde-type capillary viscometer immersed in a water bath was used to obtain inherent viscosities of the synthesized polymers by transparent thermostats (Schott, CT 72). A sampling solution was obtained through dissolution of 0.25 g of polymer in 50 mL of NMP. The inherent viscosity is determined through eqn (1) as follows:[38]

$$\eta_{inh} = \frac{\ln(t/t_0)}{c} \quad (1)$$

where $\eta_{inh}$ represents the inherent viscosity (dL $g^{-1}$), $t_0$ and $t$ are retention time of the NMP and polymer solution (s), respectively, and $c$ is concentration of the polymer solution (0.5 g $dL^{-1}$).

The physicochemical properties of the synthesized Linde T particles were analyzed *via* Brunauer–Emmett–Teller (BET) physisorption analysis, field emission scanning electron microscopy (FESEM), X-ray diffraction (XRD), Fourier transform infrared (FTIR) spectroscopy and thermogravimetric analysis (TGA). The surface area of synthesized particles was examined using a BET physisorption analyzer (BELSORP Mini II). The samples were degassed for 24 h in vacuum before measurement. FESEM (Zeiss Supra 55 VP operated at 10 kV) was employed to monitor the morphology and particle size of Linde T. Prior to analysis, a double-sided carbon tape was used to ensure the crystals were adhered to the top of the holder. A Bruker (USA) D8 Advance diffractometer equipped with a Cu Kα radiation source at a wavelength of 1.54059 Å was utilized to examine the crystalline structure of the crystals. The XRD pattern was acquired in the 2 theta range of 5°–30° with a step size of 0.02°. The chemical functionalities of Linde T particles were investigated *via* FTIR analysis using a PerkinElmer Spectrum One. The particles in powder form were homogenized with potassium bromide (KBr) before being compressed into pellet form at 10 MPa. The analytical technique was performed in transmittance mode, which ranged from 400 $cm^{-1}$ to 4000 $cm^{-1}$, using 50 scans, during which the temperature was maintained constant at room temperature. With regards to the thermal stability of Linde T particles, they were examined utilizing a PerkinElmer STA6000 TGA instrument. 15–20 mg of sample was positioned on an alumina pan prior to heating under air environment at a rate of 10°C $min^{-1}$ from 50 °C to 800 °C.

In addition, the fabricated membranes were also analyzed by FESEM, energy dispersive X-ray (EDX), XRD, attenuated total reflection (ATR) FTIR spectroscopy, TGA and differential scanning calorimetry (DSC). The phase structure of membranes was determined by cutting the membrane samples into small portions and inspecting using XRD, adopting identical parameters to those used for the Linde T particle analysis as formerly explained. In addition, FESEM and EDX were employed to evaluate the morphology of the developed membranes through obtaining images of cross-sectional views and investigation of elemental compositions of the resultant membranes respectively. Cross sections of the membranes were obtained by submerging the samples in liquid nitrogen for several minutes before fracturing the film in order to prevent morphology distortion. All the membrane samples were subsequently sputter-coated with platinum using a Quorum Q150R S coater under vacuum condition for 60 s prior to imaging. The coating process was aimed at impeding charging of the membrane sample which could happen during analysis. In addition, the elemental compositions and distributions of Linde T particles in the membranes were ascertained using Oxford Instrument Inca (EDX).

Thermal stability of the membranes was investigated using TGA with the same instrument as described for Linde T particle analysis. For DSC, a TA Instruments DSC Q2000 was utilized to measure the glass transition temperature ($T_g$) of membrane samples. Two heating regimes were employed, which were (1) increasing the temperature at a heating rate of 10 °C $min^{-1}$ to up to 450 °C under nitrogen environment and (2) initially quenching at a rate of 10°C $min^{-1}$ followed by reheating at 10°C $min^{-1}$ to complete the second heating run. The first cycle was conducted to erase all previous thermal history as well as to relax any molecular orientation captured during membrane formation. On the other hand, the second cycle of heating was used to obtain $T_g$ profiles of the membrane samples. The functional groups in the membranes were investigated using FTIR spectroscopy operated in the ATR mode equipped with a diamond crystal, with 50 scans in the wavelength range of 650–4000 $cm^{-1}$ in the transmission mode.

### 2.7 Biogas permeation measurements

The membrane samples were examined for biogas permeation including $CO_2$ and $CH_4$ single gas permeation and mixed gas comprising $CH_4$ and $CO_2$ at 30 °C and 3.5 bar by using an in-house gas permeation test rig. A detailed explanation pertaining to the setup of the permeation rig has been outlined in our previous work.[39] The temperature and pressure were set based upon common operating conditions reported in the literature for ease of comparison.

For each run, a membrane with effective area of 1.77 $cm^2$ was mounted onto the membrane test cell. To ensure reproducibility, at least 3 membrane films were tested for gas permeation data, which were obtained from 3 independently cast membranes respectively. Before each permeation test, the film was vacuumed overnight after the membrane was placed onto the test cell. This was aimed at fully degassing the system before proceeding with the experiment in order to ensure high accuracy of the obtained data. The procedures for biogas permeation testing were repeated three times in order to evaluate the repeatability of the gas separation performance of the membrane. The permeabilities of $CH_4$ and $CO_2$ single gases were then calculated through eqn (2), as follows:[40]

$$P_A = \frac{V_p t}{A_m(p_h - p_l)} \quad (2)$$

where $P_A$ refers to the gas permeability (Barrer), $V_p$ is the permeate flow rate ($cm^3$(STP) $s^{-1}$), $t$ designates the membrane thickness (cm), $A_m$ is the membrane area ($cm^2$), $p_h$ and $p_l$ are the pressures in feed side and permeate side (cmHg), respectively, and subscript A is $CO_2$ or $CH_4$. The permeability of the membrane is represented in the unit of Barrer (1 Barrer = $1 \times 10^{-10}$ $cm^3$(STP) cm $s^{-1}$ $cm^{-2}$ $cmHg^{-1}$).

The ideal selectivity of the membrane was calculated using eqn (3) as follows:[41]

$$\alpha_{CO_2/CH_4} = \frac{P_{CO_2}}{P_{CH_4}} \quad (3)$$

where $\alpha$ specifies the ideal selectivity of $CO_2/CH_4$ and $P$ refers to the permeability (Barrer).

The membrane with optimum separation performance in single gas permeations was further tested in mixed biogas separation and plasticization study. To perform $CO_2$ plasticization study, $CO_2$ permeability was examined through incremental feed pressure which was periodically elevated from 3.5 to 25 bar. Since the current study addresses high-pressure conditions, non-ideal gas effects should be considered. The driving force for this case is described as the distinction in fugacity from the high to low end across the membrane. A non-ideal equation of state has been employed to compute fugacity of $CO_2$ through adaptation of Thermosolver software according to the Peng–Robinson equation of state.[42,43] Thus, the permeability of $CO_2$ was determined based on eqn (4) as follows:[39]

$$P_{CO_2} = \frac{V_p t}{A_m(\Phi_h - \Phi_l)} \quad (4)$$

where $\Phi_f$ and $\Phi_p$ are the $CO_2$ fugacity in feed and permeate sides, respectively.

Furthermore, mixed biogas permeation of composite membranes was carried out using 64% $CO_2$ and 36% $CH_4$ mixtures at temperature and pressure of 30 °C and 3.5 bar, respectively. In this test, the feed, permeate and retentate gas streams were injected into a gas chromatograph, PerkinElmer model 2103, which was furnished with a thermal conductivity detector for composition analysis. Prior to measurement, the gas chromatograph was calibrated with known compositions of $CO_2/CH_4$ gas mixture in order to obtain the gas peak area ratio as a function of gas mole fractions. The permeability of $CO_2$ and $CH_4$ in biogas mixture was determined based on the eqn (5) and (6) as follows:[9]

$$P_{CO_2} = \frac{V_p y_{CO_2} t}{A_m(p_h x_{CO_2} - p_l y_{CO_2})} \quad (5)$$

$$P_{CH_4} = \frac{V_p y_{CH_4} t}{A_m(p_h x_{CH_4} - p_l y_{CH_4})} \quad (6)$$

where $P_{CO_2}$ and $P_{CH_4}$ indicate the permeability of $CO_2$ and $CH_4$, respectively, and $x$ and $y$ refer to the mole fraction of component in feed and permeate sides, respectively.

The selectivity for mixed biogas measurement was then assessed based on eqn (7) as follows:[44]

$$\alpha_{CO_2/CH_4} = \left(\frac{y_{CO_2}/y_{CH_4}}{x_{CO_2}/x_{CH_4}}\right) \quad (7)$$

## 3 Results and discussion

### 3.1 Characterization of virgin fluorinated polyimide membrane and Linde T-based composite membranes

**3.1.1 Physical appearance of the membranes.** Images of virgin fluorinated polyimide membrane and Linde T/fluorinated polyimide composite membranes (S1–S5) fabricated using different filler dispersion durations are shown in Fig. 2. It can be observed from Fig. 2 that all the membranes are transparent, which demonstrates no phase separation phenomenon happens during the fabrication process. In addition, although all membranes were prepared at varying filler dispersion durations, they are able to bend as well as exhibit excellent characteristics, such as being resilient, non-brittle and flexible regardless of their fabrication procedure.

**3.1.2 Surface area and morphology analysis.** For BET analysis, the synthesized Linde T particles demonstrate surface area and micropore volume of 21.60 $m^2$ $g^{-1}$ and 0.006 $cm^3$ $g^{-1}$, respectively, which are in good agreement with values reported in the literature.[45] The FESEM image of Linde T particles is shown in Fig. 3(b). Based on Fig. 3(b), it can be seen that Linde T particles exhibit a typical rod-like structure with average particle size of 3.9 μm, which is consistent with the morphology of Linde T reported by Rad *et al.*[46] The size of Linde T crystals was measured based on the average length of 50–55 Linde T rods. The standard deviation obtained was approximately 0.35, which confirmed that the Linde T crystals were uniformly distributed.

Fig. 4 and 5 show the cross-section and bottom-layer images of the resultant Linde T/fluorinated polyimide composite

 

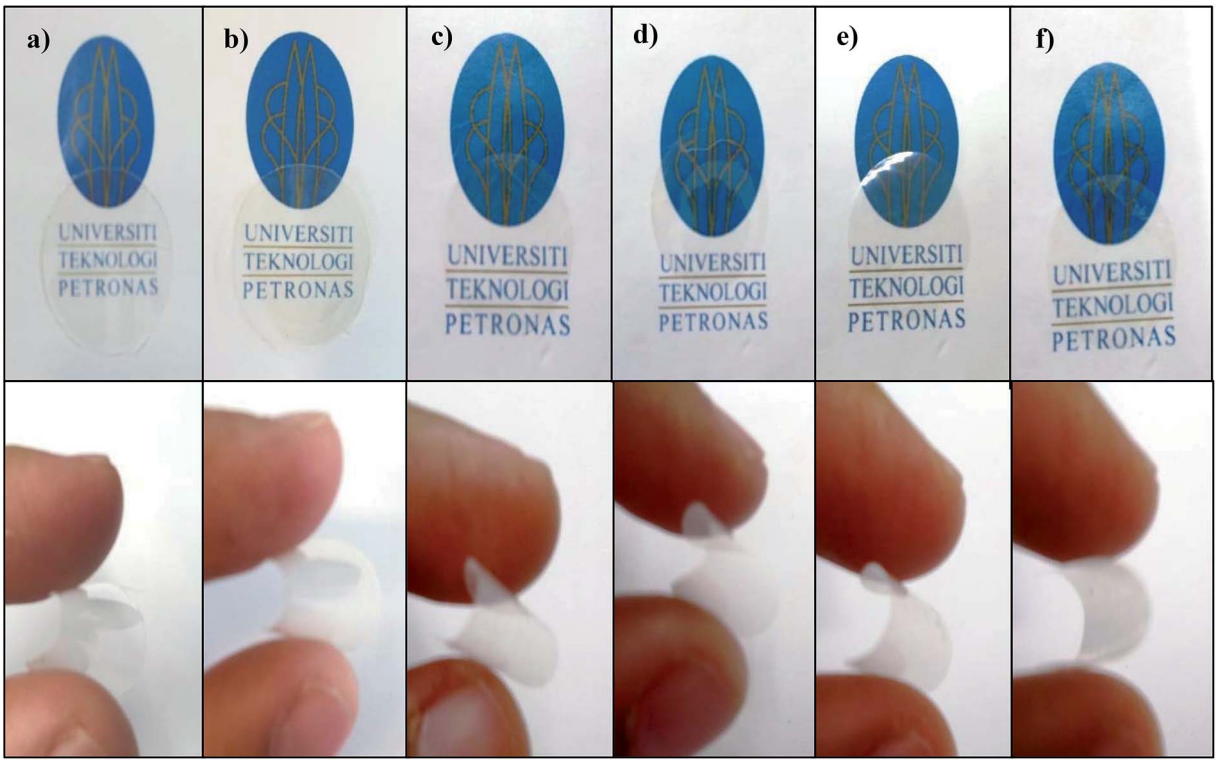


Fig. 2 The physical appearance of (a) virgin fluorinated polyimide membrane and Linde T/fluorinated polyimide composite membranes fabricated at different filler dispersion durations: (b) S1, (c) S2, (d) S3, (e) S4 and (f) S5.

membranes fabricated using different fabrication parameters, respectively. Meanwhile, Fig. 6 demonstrates the EDX mapping from the cross sections of the membranes. Since Linde T particles mainly consist of silicon element, the EDX analysis was conducted by mapping the occurrence of Si element in the membranes, which is representative of the distribution of Linde T particles in the polymer phase. Referring to Fig. 4 and 5, the FESEM images of all the composite membrane samples demonstrate that the Linde T crystals are embedded in the fluorinated polyimide phase.

Based on the FESEM image of S1 sample in Fig. 4(a), it is revealed that Linde T particles are uniformly dispersed in the polymeric matrix. This suggests that an excellent compatibility between Linde T and fluorinated polyimide phase has been

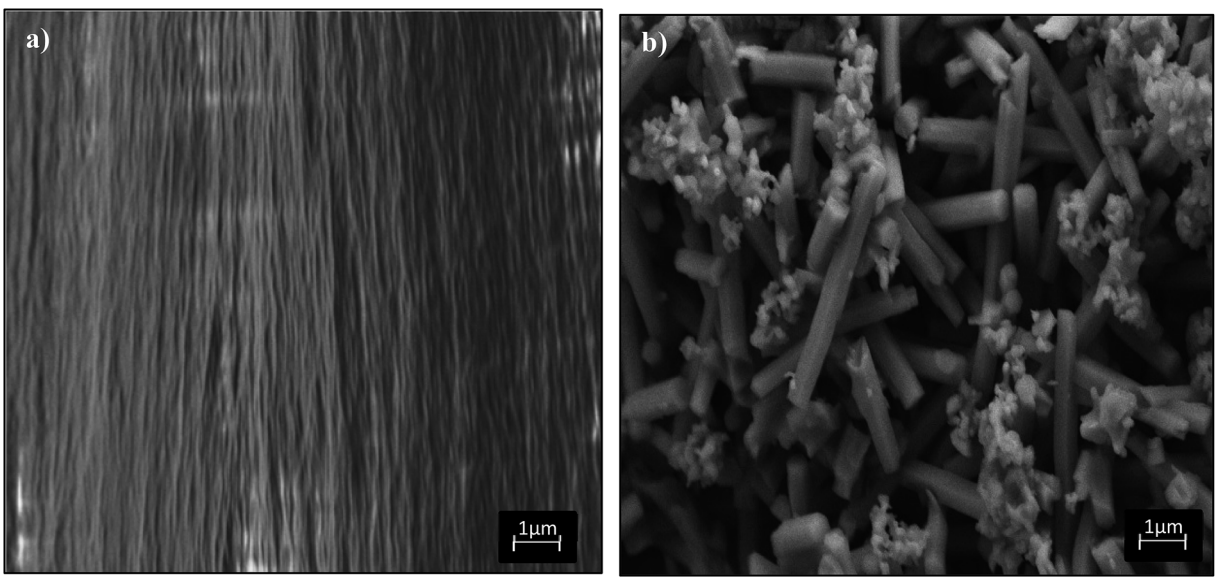


Fig. 3 FESEM images of (a) virgin fluorinated polyimide membrane and (b) Linde T crystals prepared in the current research.

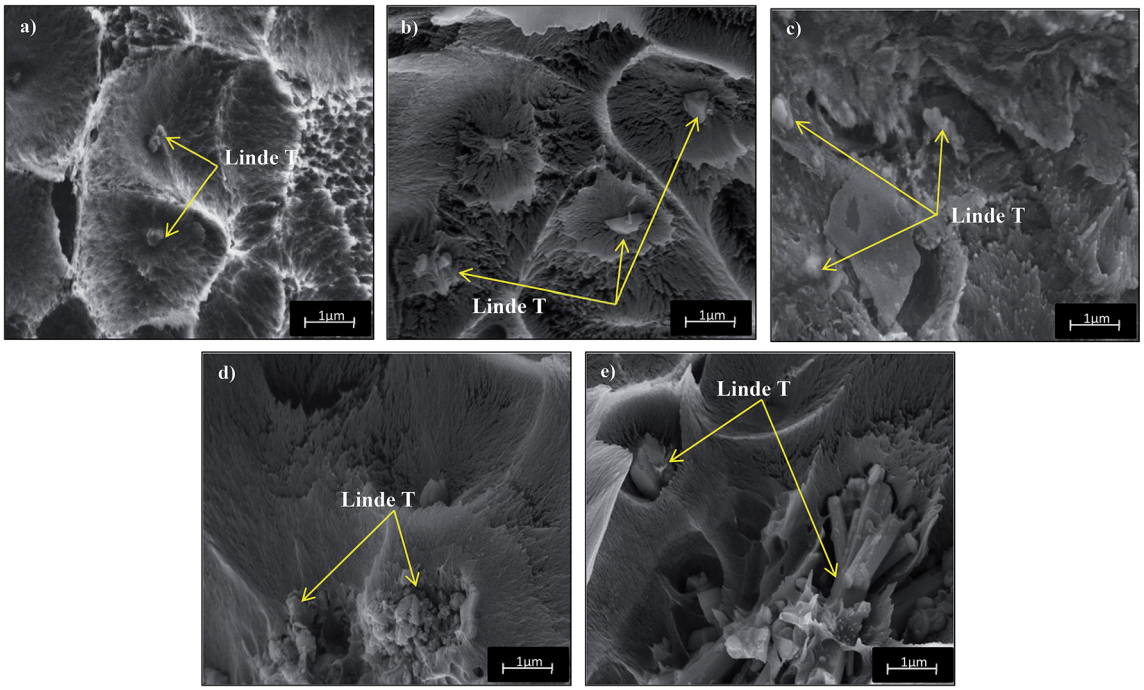


Fig. 4 Cross-section images of Linde T/fluorinated polyimide composite membranes fabricated with different filler dispersion durations: (a) S1, (b) S2, (c) S3, (d) S4 and (e) S5.

attained. This finding was further confirmed by the homogeneous dispersion of Si element in EDX mapping as demonstrated in Fig. 6(a). Nevertheless, as the duration of filler dispersion rises from 2 h to 4 h (S2), the FESEM image of S2 membrane in Fig. 4(b) exhibits the occurrence of small-scale particle clumping phenomenon due to the aggregation of Linde T particles in the polymeric phase. The existence of void space between Linde T particles and fluorinated polyimide matrix is also not pronounced in the resultant membrane. Even though formation of voids and sedimentation are not found in

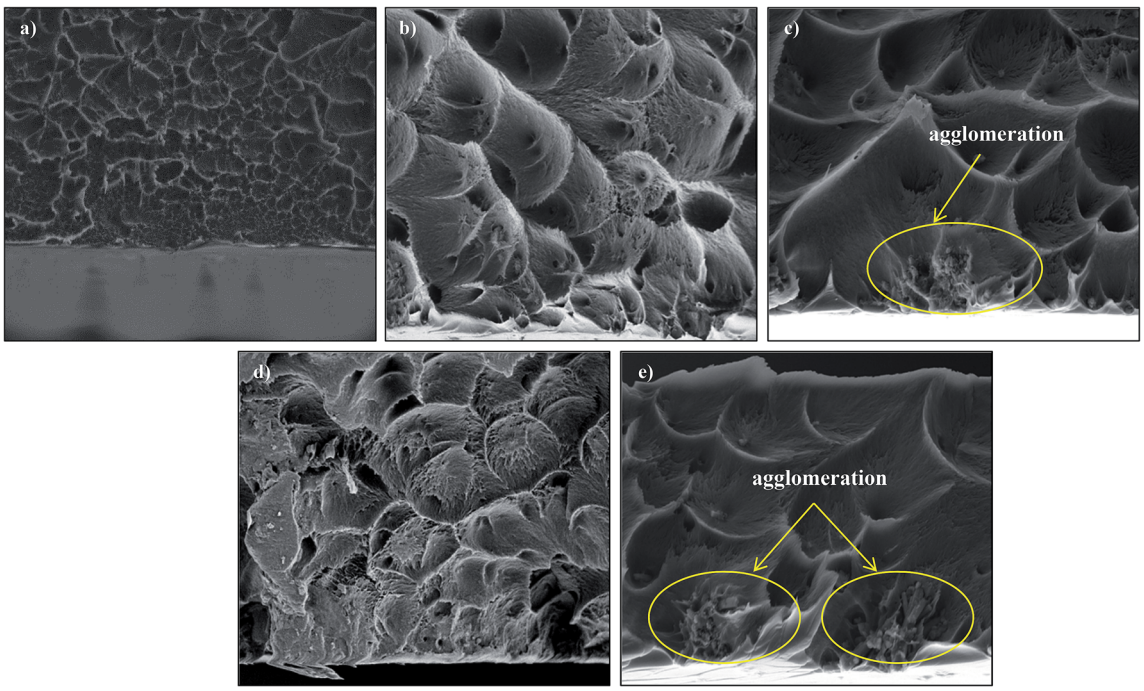


Fig. 5 Bottom-layer FESEM images of Linde T/fluorinated polyimide composite membranes fabricated with different filler dispersion durations: (a) S1, (b) S2, (c) S3, (d) S4 and (e) S5.

 

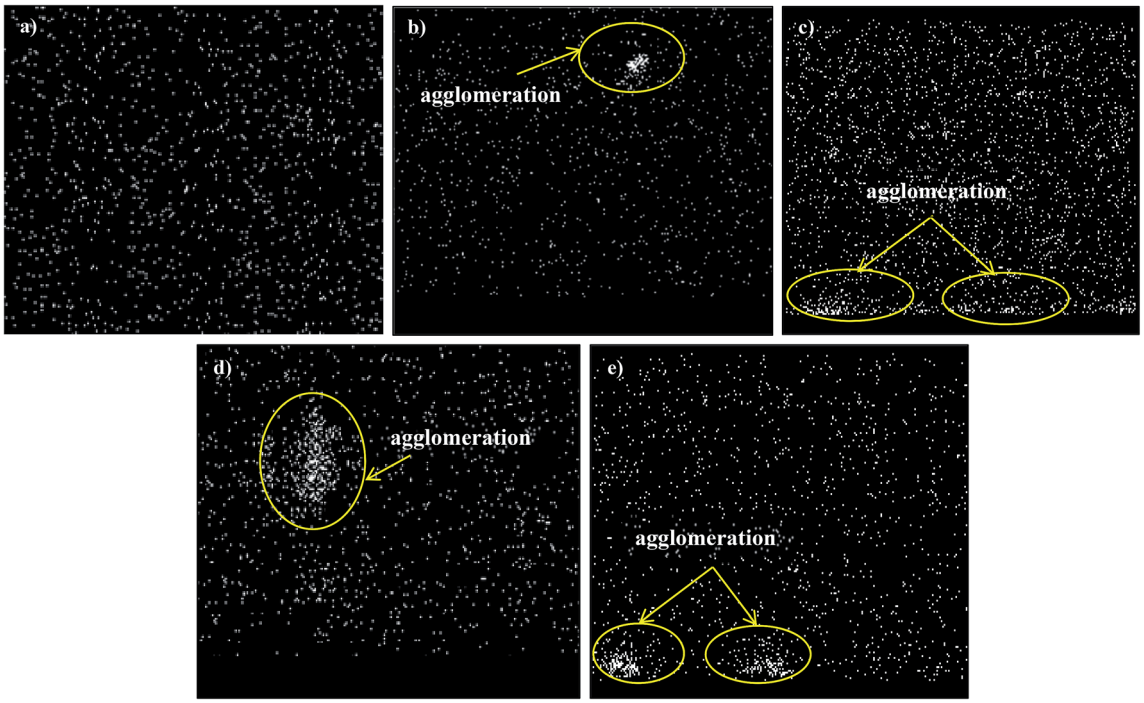


Fig. 6 EDX mapping for Si element from the cross sections of Linde T/fluorinated polyimide composite membranes: (a) S1, (b) S2, (c) S3, (d) S4 and (e) S5.

the FESEM images shown in Fig. 4 and 5, slight agglomeration of Linde T particles in the polymer matrix can be seen in the EDX mapping image in Fig. 6(b). The minor agglomeration of Linde T particles in S2 membrane is anticipated because of the ripening effect, which is attributed to sonication during membrane fabrication. During the course of sonication, the collapse of cavitation bubbles leads to shockwave impacts and interparticle collisions that can lead to particle breakage and particle size reduction.[47] Subsequently, this phenomenon induces the dissolution of smaller particles and increase the tendency of small particles to clump together and form larger particles as an ultimate result.[48] Therefore, it is expected that two processes, sonofragmentation and Ostwald ripening, might occur simultaneously when the duration of sonication increases.[49,50]

In addition, prolonging the duration of stirring and sonication to 6 h increases the aggregation of Linde T particles with the confirmation shown in Fig. 4(c) and (d) for S3 and S4 membranes, respectively. In fact, this observation is intuitively reasonable since an increase in the duration of stirring and sonication customarily induces the formation of particle clumps and larger particles due to the ripening effect as elaborated earlier. In addition, based on EDX mapping images in Fig. 6(c) and (d), it could be observed that a small amount of Linde T particles are moved, clustered and settled at the bottom layer of S3; meanwhile, the agglomeration of Linde T particles in the polymer phase can be seen in S4. These results demonstrate a comparatively reduced particle dispersion of Linde T particles in the fluorinated polyimide phase for S3 and S4 membranes.

Nevertheless, when the filler dispersion duration increases to 8 h (S5), apparent agglomeration and sedimentation of the Linde T particles in the fluorinated polyimide polymer phase are observed with the appearance of pinholes and voids in the membrane as shown in Fig. 4(e) and 5(e). This result is evidence of heterogeneous distribution of Linde T particles in the polymer matrix, which could subsequently form channels for unselective gas transport. Furthermore, a poor dispersion of Linde T particles in the polymer matrix is further demonstrated in Fig. 6(e) through EDX mapping image. Overall, based on the results obtained, 2 h duration of filler dispersion creates better blending and homogeneity of Linde T in the polymer phase than the longer durations of stirring and sonication.

**3.1.3 Crystallinity and functional group analysis.** The XRD patterns for Linde T particles and virgin fluorinated polyimide membrane synthesized in the current work as well as reported in the literature in the $2\theta$ range of 5° to 28° are shown in Fig. 7. Referring to Fig. 7(a), the XRD pattern for Linde T particles is in agreement with results reported in the literature, as shown in Fig. 7(b) for Linde T structure, with characteristic peaks at $2\theta$ values of 7.7°, 13.5°, 20.5°, 23.5° and 24.8°.[51] This finding proved the formation of crystalline Linde T phase. In addition, a sharp peak at $2\theta$ of 7.7° was seen in the XRD pattern of Linde T, demonstrating a successful attainment of highly crystalline structure. Referring to Fig. 7(a) also, the XRD pattern of virgin fluorinated polyimide membrane demonstrates a broad peak from 8° to 22°, which indicates the amorphous structure characteristic for the polymer phase. This result corresponded well with the reported XRD pattern for fluorinated polyimide membrane shown in Fig. 7(b).[14,52] However, the XRD patterns of

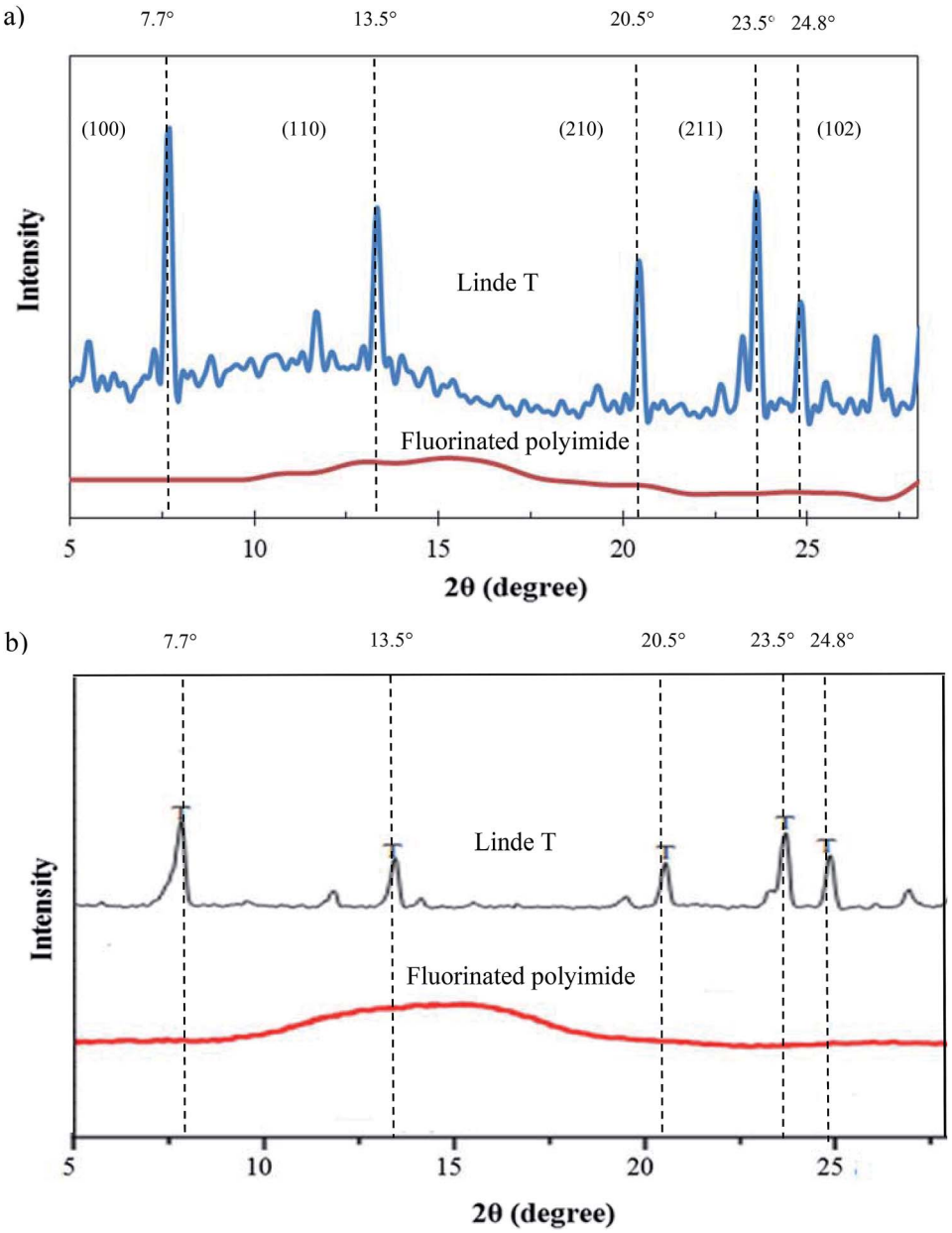


Fig. 7 XRD patterns of Linde T particles and virgin fluorinated polyimide membrane (a) fabricated in the current work and (b) reported in the literature.[53,54]

Linde T/fluorinated polyimide composite membranes fabricated at different filler dispersion durations are not discussed since the peaks of Linde T particles are not prominent, which might be ascribed to the low amount of Linde T particles (1 wt%) embedded in the polymer phase.[53]

Fig. 8 demonstrates the FTIR spectrum of Linde T particles and ATR-FTIR spectra for virgin fluorinated polyimide and Linde T-based composite membranes fabricated at different filler dispersion durations. Based on Fig. 8, Linde T particles demonstrate characteristic peaks at 720–775 $cm^{-1}$ and 1040–1150 $cm^{-1}$. The peaks in the region of 720–775 $cm^{-1}$ represent the symmetric stretching vibrations of double ring for the Linde T structure.[54] On the other hand, asymmetric stretching vibrations are characterized by the peaks at 1040–1150 $cm^{-1}$.[55] The characteristic peaks of Linde T particles observed in this research were in good accordance with FTIR result revealed for Linde T structure in the published literature.[56]

Meanwhile, it can be observed from Fig. 8 that the ATR-FTIR spectrum for virgin fluorinated polyimide membrane exhibits peaks at 718 $cm^{-1}$, 1250 $cm^{-1}$, 1352 $cm^{-1}$, 1715 $cm^{-1}$ and 1785 $cm^{-1}$. The peak at 718 $cm^{-1}$ is attributed to the imide ring or the imide carbonyl group. Meanwhile, imide group C–N stretch and C–F stretch in $CF_3$ group are characterized by the peaks at 1352 $cm^{-1}$ and 1250 $cm^{-1}$, respectively. In addition, the C=O symmetric and asymmetric stretch of imide group are indicated by the bands at 1715 $cm^{-1}$ and 1785 $cm^{-1}$,

 

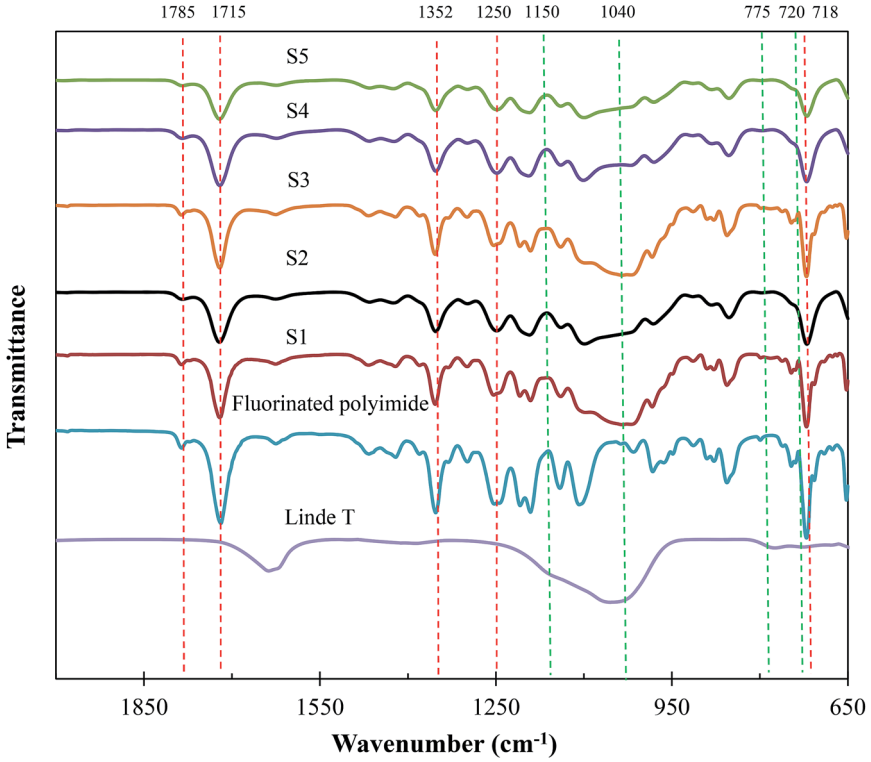


Fig. 8 ATR-FTIR analysis of Linde T particles, virgin fluorinated polyimide membrane and Linde T/fluorinated polyimide composite membranes fabricated at different filler dispersion durations (S1–S5).

respectively. The characteristic peaks of fluorinated polyimide membrane are in agreement with those IR peaks recorded in the literature for the fluorinated polyimide structure.[34,57,58]

On the other hand, the spectra of the composite membranes exhibit the characteristics of both Linde T and fluorinated polyimide with no apparent changes in absorption bands as compared to the Linde T particles and virgin fluorinated polyimide membrane. This outcome demonstrates that the fabrication of composite membranes at different filler dispersion durations did not alter the interaction between functional groups of Linde T particles and polymer matrix in the resultant composite membranes.

**3.1.4 Thermal stability and glass transition temperature analysis.** The weight losses of Linde T particles, virgin fluorinated polyimide membrane and the Linde T/fluorinated polyimide composite membranes fabricated at different filler dispersion durations were obtained using TGA under air environment, and the TGA plots and decomposition temperatures of the membranes are shown in Fig. 9 and Table 2, respectively. Based on Fig. 9, ~10 wt% weight loss within the temperature range of 80 °C to 200 °C is observed in the TGA curve for Linde T particles, which is explained through removal of moisture content confined in Linde T.[59] When the temperature was further increased up to 800 °C, the total weight loss for Linde T particles was 14.9 wt%. Meanwhile, virgin fluorinated polyimide membrane shows thermal stability up to 500 °C, which matches well with the profile reported by Shao *et al.*[60] and Lin *et al.*[58] for fluorinated polyimide membrane. The decomposition of virgin fluorinated polyimide membrane might involve the complete degradation of polymer matrix including nitrogen and carbon.[61]

Based on Fig. 9 and Table 2, all the composite membranes (S1–S5) displayed thermal stability up to ~500 °C. The decomposition of the composite membranes is contributed by Linde T particle framework and fluorinated polyimide matrix. A rapid weight loss between 500 °C and 600 °C is noticed by virtue of the decomposition of fluorinated polyimide polymer. In addition, all the prepared composite membranes (S1–S5) demonstrate minor shifts in the decomposition temperature (~515–519 °C). This finding indicates that prolonging the filler dispersion duration from 2 h to 8 h did not influence the thermal stability of the membrane. In addition, it is also observed that the changes in final weight residues of the membranes are negligible. This is mainly due to the similar loading of Linde T particles (1 wt%) amalgamated into the fluorinated polyimide polymer for all the membranes.

The DSC curves and glass transition temperatures ($T_g$) of the resultant membranes are shown in Fig. 10 and Table 2, respectively. The average $T_g$ value of each membrane was obtained by conducting at least 3 measurements. The standard deviation of the acquired $T_g$ values from DSC measurements was about ±1 °C. Referring to Fig. 10 and Table 2, the $T_g$ of virgin fluorinated polyimide membrane is 410 °C, which is in good agreement with the reported literature data.[14] Meanwhile, all composite membranes show greater $T_g$ value of up to 425 °C than the virgin membrane, indicating that the Linde T particles

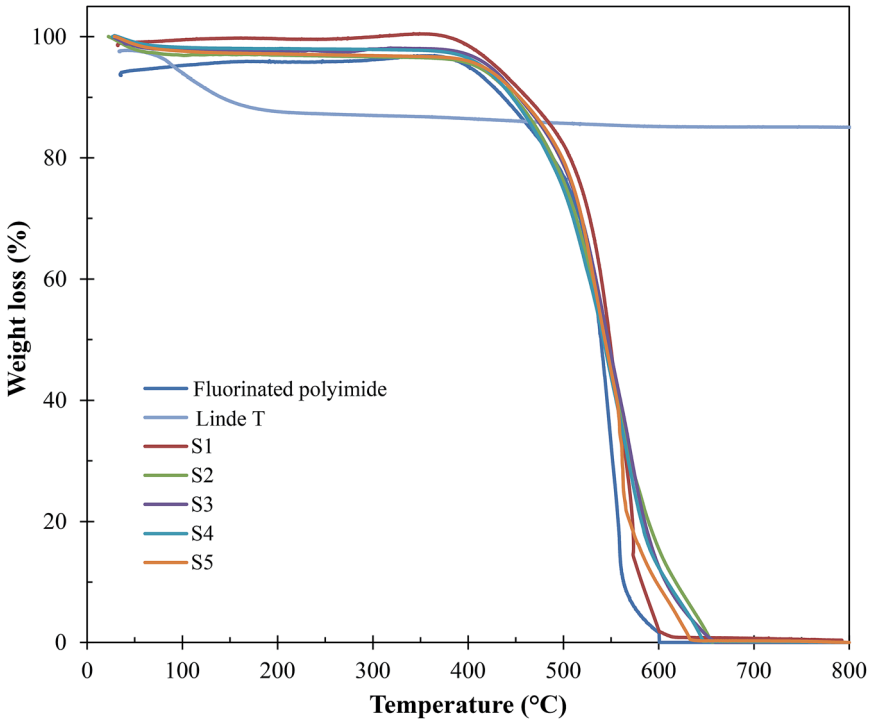


Fig. 9 TGA curves of Linde T particles, virgin fluorinated polyimide membrane and Linde T/fluorinated polyimide composite membranes fabricated at different filler dispersion durations (S1–S5).

Table 2 Thermal glass transition temperature of virgin fluorinated polyimide membrane and composite membranes fabricated at different filler dispersion durations (S1–S5)

| Membrane | Decomposition temperature, $T_d$ (°C) | Glass transition temperature, $T_g$ (°C) |
|---|---|---|
| Virgin fluorinated polyimide | 512.50 | 410 |
| S1 | 518.75 | 425 |
| S2 | 515.10 | 423 |
| S3 | 516.20 | 420 |
| S4 | 515.63 | 420 |
| S5 | 515.95 | 420 |

have altered the packing structure of the polymer membrane. When the total stirring and sonication duration is enhanced from 2 h to 8 h, the value of $T_g$ decreases from 425 °C to 420 °C (S1–S5), signifying an increase of polymer chain flexibility and a reduction in membrane rigidity.[62]

### 3.2 Biogas permeation tests

Fig. 11 and 12 show the $CH_4$ and $CO_2$ permeabilities and $CO_2/CH_4$ selectivities of the resultant membranes, respectively, which are critical elements in biogas upgrading. Referring to Fig. 11, all the resultant composite membranes display greater $CO_2$ permeability and smaller $CH_4$ permeability in comparison to the virgin fluorinated polyimide membrane. The composite membranes demonstrate $CO_2$ permeability of 843.60 Barrer, 670.72 Barrer, 631.21 Barrer, 646.64 Barrer and 690.95 Barrer for S1, S2, S3, S4 and S5, respectively, while a $CO_2$ permeability of 468.01 Barrer is exhibited by the virgin membrane. With respect to $CH_4$ permeability, all the composite membranes, except S5, exhibit a lower value in comparison to the virgin fluorinated polyimide membrane. Moreover, viewing from the aspect of $CO_2/CH_4$ selectivity as shown in Fig. 12, all the composite membranes demonstrate higher values ranging from 10.3 to 19.1 than the virgin fluorinated polyimide membrane with a selectivity of only 7.03.

The improved gas performance of the composite membranes prepared in this research is mainly attributed to the incorporation of Linde T particles in the fluorinated polyimide polymer phase. The inclusion of Linde T particles affects the polymer chain packing and subsequently boosts the free volume that acts as pathway for diffusion of gas penetrants.[38] Moreover, the gas permeation of the Linde T/fluorinated polyimide composite membranes could be enhanced by the presence of Linde T pores (0.36 nm × 0.51 nm), which allow passage of $CO_2$ with smaller kinetic diameter (3.3 Å) compared to the larger kinetic diameter of $CH_4$ (3.8 Å).[63] Thus, it can be stated that the presence of Linde T particles in fluorinated polyimide enhanced the diffusivity of gas and subsequently improved the $CO_2$ gas permeability of the resultant composite membranes. On the other hand, the enhancement of $CO_2/CH_4$ separation performance might be attributed to $CO_2$ adsorption coverage on Linde T pore walls. In addition, $CO_2$ may be transported with less restriction through the Linde T pores since Linde T surface can promote greater electrostatic interaction with $CO_2$ in comparison with $CH_4$.[63,64] Furthermore, the existence of hexafluoropropane linkage in fluorinated polyimide might also lead to limited rotation of

 

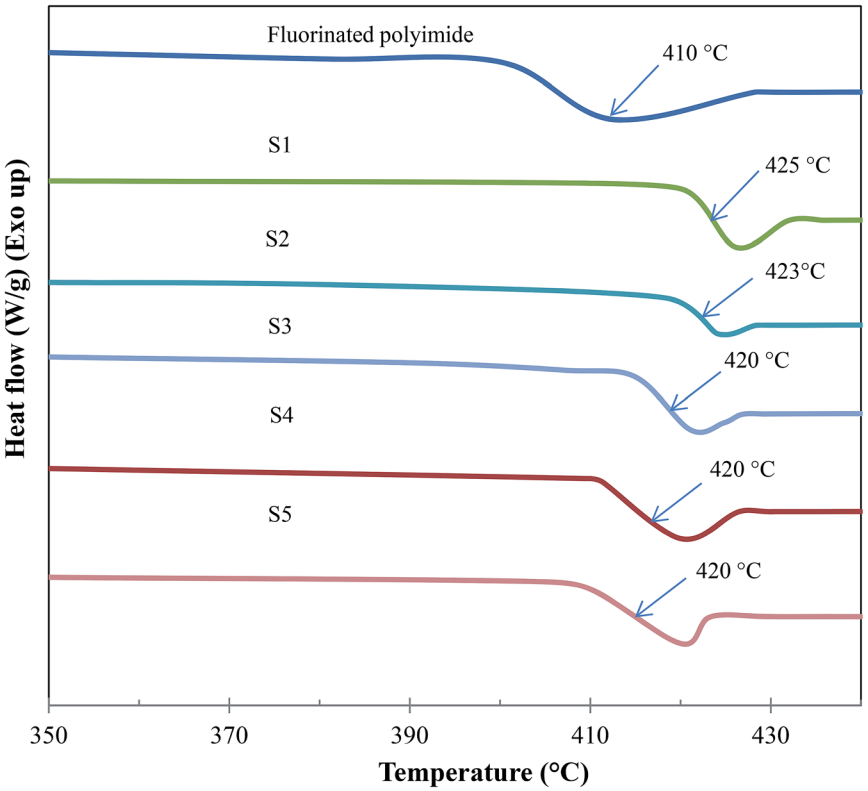


Fig. 10 DSC curves of virgin fluorinated polyimide membrane and composite membranes fabricated at different filler dispersion durations (S1–S5).

neighboring phenyl rings, augmenting interaction with non-polar $CO_2$ and stiffer backbones, which subsequently all resulted in enhanced gas separation performance.[65]

Furthermore, it can be observed from Fig. 11 that the enhancement of filler dispersion duration from 2 h (S1) to 8 h (S5) leads to a decrease in $CO_2$ permeability from 843.60 Barrer

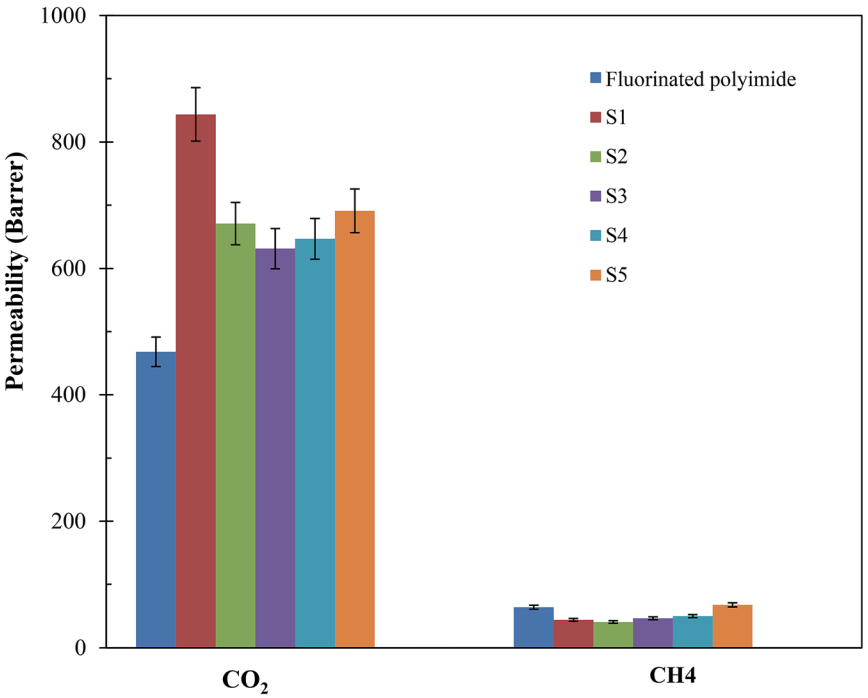


Fig. 11 $CO_2$ and $CH_4$ permeabilities of virgin fluorinated polyimide membrane and Linde T/fluorinated polyimide composite membranes fabricated with different filler dispersion durations (S1–S5) at a temperature of 30 °C and pressure of 3.5 bar.

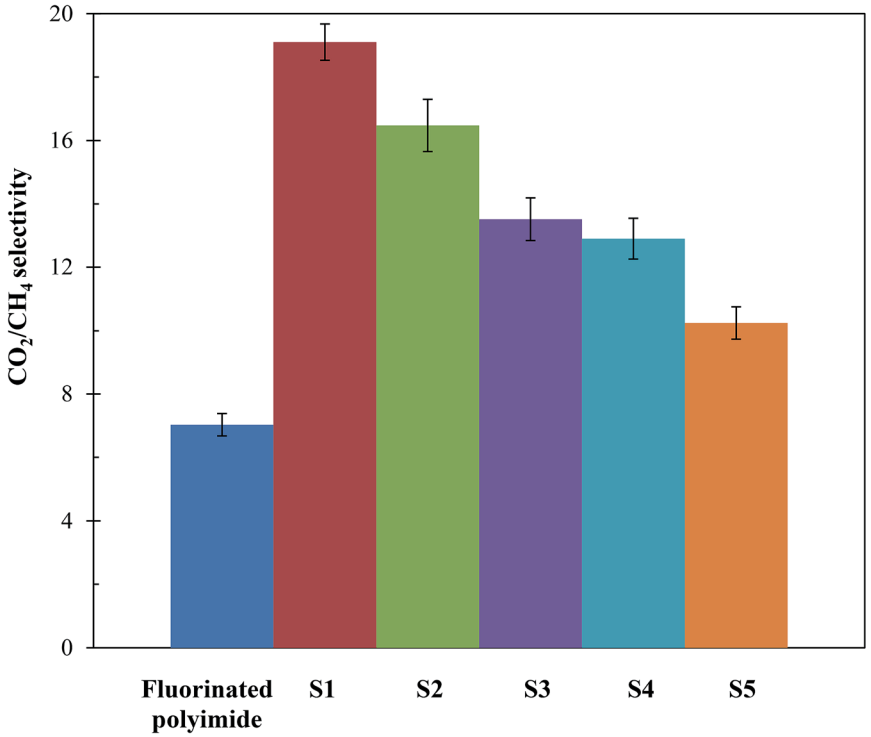


Fig. 12 $CO_2/CH_4$ selectivity of virgin fluorinated polyimide membrane and Linde T/fluorinated polyimide composite membranes fabricated with different filler dispersion durations (S1–S5) at a temperature of 30 °C and pressure of 3.5 bar.

to 670.72 Barrer. Meanwhile, the shortest stirring and sonication duration of 2 h (S1) also leads to the greatest advancement in terms of $CO_2$ permeability and $CO_2/CH_4$ selectivity. In comparison to the virgin fluorinated polyimide membrane, S1 membrane displayed 80% increase in $CO_2$ permeability and 44% reduction in $CH_4$ permeability, while an improvement of $CO_2/CH_4$ selectivity of as high as 172% is attained. The improvement in $CO_2$ permeability and $CO_2/CH_4$ selectivity of S1 is also confirmed through EDX mapping and FESEM images as demonstrated in Fig. 4–6, whereby a good dispersion of Linde T particles and absence of interfacial voids between polymer phase and particles were observed for S1. In addition, as shown in Table 2, the highest $T_g$ value is also obtained for S1 membrane, which is associated with its higher gas separation performance.[66] The increase of $T_g$ can be linked to the enhancement of microvoid formation, which leads to the increase of permeability. Furthermore, the improvement of permeability with regards to $T_g$ can also be explained by using eqn (8), where $T_g$ is directly proportional to permeability:[66]

$$\log P = (a_p/T_g) + b_p \quad (8)$$

where $P$ refers to the permeability (Barrer), $a_p$ and $b_p$ are the values of the constants for the gases and $T_g$ indicates the glass transition temperature (K). The values of $a_p$ and $b_p$ for $CO_2$ are −778 K and 3.29, respectively. Meanwhile, the values of $a_p$ and $b_p$ for $CH_4$ are −1410 K and 4.08, respectively.

Moreover, the enhancement of $T_g$ also signifies the reduction of polymer chain flexibility, for which the increase of chain rigidity leads to a greater difference between the diffusion coefficients of smaller, $CO_2$, and larger, $CH_4$, penetrants. Consequently, $CO_2/CH_4$ selectivity improved. Nevertheless, prolonging the duration of filler dispersion from 2 h to 8 h contributed to the improvement of $CH_4$ permeability from 44.16 Barrer to 67.43 Barrer, respectively. This could be due to presence of pinholes and significant agglomeration of Linde T particles within the polymeric phase, which ultimately lead to permeation of $CH_4$ with greater critical size through the membrane matrix.

Besides that, it is observed in Fig. 11 and 12 that membranes fabricated with longer filler dispersion durations (S2–S5) display reduced $CO_2$ permeability and $CO_2/CH_4$ selectivity relative to S1. The decrease of permeability might be due to partial pore blockage of filler by polymer chains.[12] Although it is not easy to block Linde T pores with polymeric chains, it may potentially affect a portion of the pores by covering the particle surfaces.[62,67] In addition, the decrease in selectivity might be because of the existence of voids occluded by the agglomerates of Linde T particles, as shown in Fig. 4–6, which reduces the gas separation performance as an end observation. Thus, in the current research, it can be summarized that a stirring and sonication duration of 2 h is the optimum filler dispersion period for fabricating Linde T/fluorinated polyimide composite membranes for $CO_2/CH_4$ separation performance, which resulted in $CO_2$ permeability of 843.6 Barrer, $CH_4$ permeability of 44.2 Barrer and $CO_2/CH_4$ selectivity of 19.1.

### 3.3 Mixed biogas permeation measurement and $CO_2$-induced plasticization resistance tests

Since sample S1 showed the optimal single gas permeation performance among the composite membranes, mixed biogas

 

Table 3 Pure and mixed gas (64 vol% $CO_2$/36 vol% $CH_4$) permeation properties of Linde T/fluorinated polyimide composite membrane at a temperature of 30 °C and pressure of 3.5 bar

| | Permeability | | |
|---|---|---|---|
| Measurement | $CO_2$ | $CH_4$ | $CO_2/CH_4$ selectivity |
| Pure gas | 843.6 | 44.2 | 19.1 |
| Mixed gas | 582.4 | 48.6 | 12.0 |

permeation and $CO_2$-induced plasticization tests of up to 25 bar were conducted using that membrane. Table 3 demonstrates the permeability and selectivity for biogas using sample S1. The fabricated membrane successfully removed >96% of $CO_2$ from the mixed biogas. Thus, this membrane has a great potential in upgrading biogas to biomethane as a renewable substitute for natural gas. Based on Table 3, S1 membrane displays higher gas separation performance under single gas condition as compared to mixed biogas measurement. The reduction in permeability and selectivity in mixed biogas condition is anticipated because of the competitive effect between $CO_2$ and $CH_4$ penetrants in mixed gas. Moreover, the $CH_4$ may occupy the pore apertures of Linde T and subsequently impede the movement of $CO_2$ in penetrating through the membranes.[68] Furthermore, it could also be attributed to gas polarization effect and non-ideality of gas phase.[69]

Furthermore, membranes with antiplasticization attribute are vital in order to maintain a consistent promising separation performance over long service periods, and therefore a $CO_2$-induced plasticization test was conducted. Fig. 13 shows the curves of $CO_2$-induced plasticization of virgin fluorinated polyimide and S1 membranes. Based on Fig. 13, it can be noticed that $CO_2$ permeability of virgin fluorinated polyimide membrane declines with increasing pressure up to 5 bar. The lowest $CO_2$ permeability of the virgin membrane at 5 bar indicates its plasticization pressure.[70] On the other hand, the permeability of $CO_2$ starts to increase when the pressure is further increased above the plasticization pressure because local segmental motion promoted by the plasticizing agent, $CO_2$, loosens free chains.[71]

The S1 membrane demonstrates a similar decrease in $CO_2$ permeability with increasing pressure up to 20 bar. Obviously, the incorporation of Linde T into the fluorinated polyimide polymer matrix has successfully enhanced the resistance to $CO_2$ plasticization of up to 300% compared to the virgin fluorinated polyimide membrane of merely 5 bar. This improvement might be attributed to greater molecular interactions between the particles and polymer phase that reduce the likelihood of polymeric chains slipping over each other with sorption of $CO_2$ since they are held more tightly together. Furthermore, the increase in plasticization resistance might be due to the reinforcement and constraining effect of the rigid Linde T particles on molecular movement of polymeric chains.[72] Incorporation of particles within the polymeric matrix may limit the flexibility of the polymer, which further increases the $CO_2$ plasticization pressure of resulting composite membranes, which has been supported as well in previously published literature.[73]

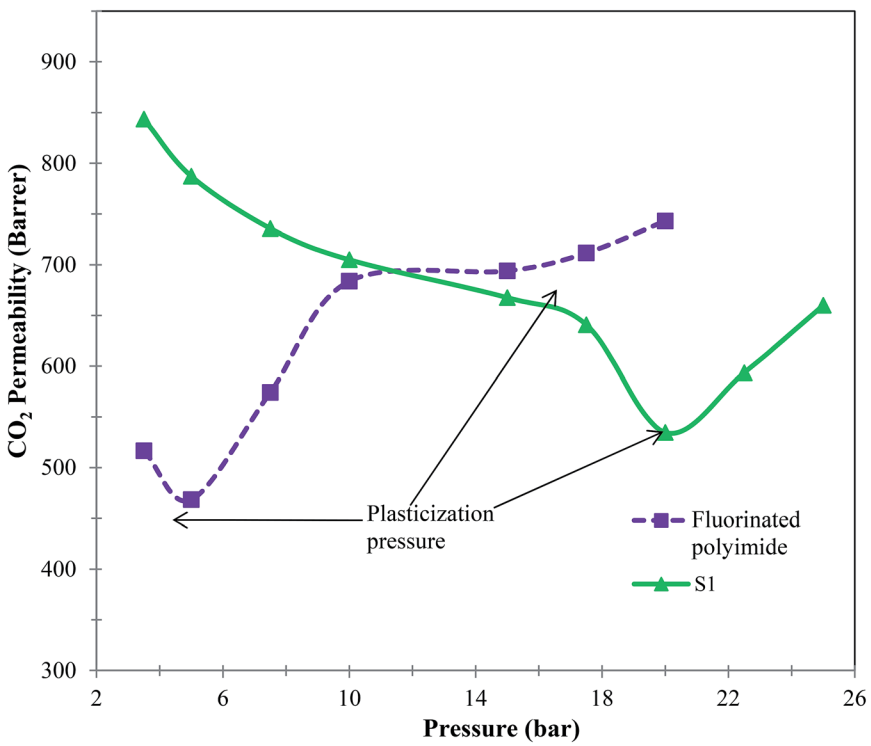


Fig. 13 $CO_2$-induced plasticization behavior of virgin fluorinated polyimide membrane and Linde T/fluorinated polyimide composite membrane at a temperature of 30 °C.

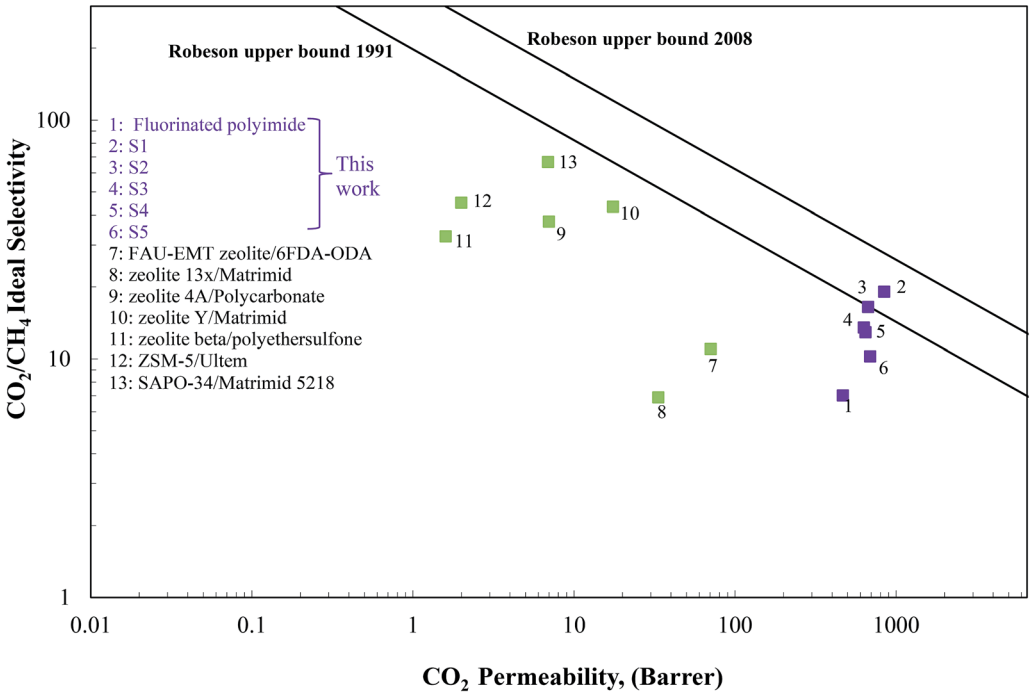


Fig. 14 Gas separation performance of Linde T/fluorinated polyimide composite membranes compared with the $CO_2/CH_4$ Robeson upper bounds.

### 3.4 Comparison of fabricated composite membranes with literature data

The separation performance of the Linde T/fluorinated polyimide composite membranes in the present work was compared with the Robeson upper bound limit, with the results being summarized in Fig. 14. As illustrated in Fig. 14, it can be observed that the performance of the virgin fluorinated polyimide membrane lies below the 1991 Robeson upper bound limit.

Although the addition of Linde T in the fluorinated polyimide polymer phase has demonstrated success in increasing both $CO_2$ permeability and $CO_2/CH_4$ selectivity compared to the virgin fluorinated polyimide membrane, none of the composite membranes are able to surpass the 2008 Robeson upper bound line. However, S1 membrane successfully transcends the 1991 limit and approaches close towards the 2008 Robeson trade-off line. In addition, Fig. 14 also compares the values of $CO_2$ permeability and $CO_2/CH_4$ selectivity of the Linde T/fluorinated polyimide composite membranes with previously published literature, relating to different types of zeolite-based composite membranes.[16,22,24,74–77] Based on Fig. 14, it is shown that the composite membranes prepared in the current work show higher performance as compared to the zeolite-based composite membranes reported in the literature. This finding shows that the Linde T/fluorinated polyimide membranes are potential candidates for use in upgrading raw biogas.

## 4 Conclusions

Biogas generated from waste can be refined to biomethane as a sustainable substitute for natural gas. The utilization of membrane separation for on-site biogas purification has emerged as an interesting approach to remove $CO_2$ before commercial utilization of biomethane. In this work, composite membranes comprising Linde T and fluorinated polyimide phase were prepared using a facile fabrication method and their performance was evaluated in biogas upgrading. The results indicated that the composite membrane fabricated using 2 h of filler dispersion duration exhibited good dispersion of Linde T in the fluorinated polyimide phase without the presence of interfacial voids between fillers and polymeric matrix. In addition, the membrane displayed the highest value of $CO_2$ permeability and $CO_2/CH_4$ selectivity as compared to other membranes as well as exhibiting an increased $CO_2$ plasticization pressure of 300% compared to the virgin polyimide membrane. Furthermore, the fabricated membrane also successfully removed >96% $CO_2$, which met the biomethane quality requirement for vehicle fuel utilization. Overall, the present work has contributed significantly to the study of determining the optimized parameters for fabrication of Linde T/fluorinated polyimide composite membranes, which is vital in finding a feasible method for the fabrication of a new composite membrane. Moreover, the successful development of this membrane material is of great importance for the industrial employment of composite membranes in $CO_2$ removal, which is beneficial for the biomethane production industry.

## Conflicts of interest

There are no conflicts to declare.

 

## Acknowledgements

The technical and financial supports provided by Centre for Contaminant Control & Utilization (CenCoU) under YUTP grant (grant no. 015LCO-113) and CO2 Research Centre (CO2RES) research group, Universiti Teknologi PETRONAS are duly acknowledged.

## References

1 D. Hedberg, S. Kullander and H. Frank, *Ambio*, 2010, **39**(suppl 1), 1–10.
2 H. Ma, Y. Guo, Y. Qin and Y.-Y. Li, *Bioresour. Technol.*, 2018, **269**, 520–531.
3 M. Tabatabaei and H. Ghanavati, *Biogas Fundamentals, Process and Operation*, Springer, 2018.
4 Y.-M. Wu, J. Yang, X.-L. Fan, S.-F. Fu, M.-T. Sun and R.-B. Guo, *Bioresour. Technol.*, 2017, **231**, 124–128.
5 N. Jusoh, Y. F. Yeong, K. K. Lau and A. M. Shariff, *Procedia Eng.*, 2016, **148**, 1259–1265.
6 N. E. Joseph, Msc thesis, Teri University, 2015.
7 N. Jusoh, Y. F. Yeong, T. L. Chew, K. K. Lau and A. M. Shariff, *Sep. Purif. Rev.*, 2016, **45**, 321–344.
8 L. M. Robeson, *J. Membr. Sci.*, 2008, **320**, 390–400.
9 S. Escorihuela, L. Valero, A. Tena, S. Shishatskiy, S. Escolastico, T. Brinkmann and J. M. Serra, *Membranes*, 2018, **8**, 1–18.
10 M. Simcik, M. C. Ruzicka, M. Karaszova, Z. Sedlakova, J. Vejrazka, M. Vesely, P. Capek, K. Friess and P. Izak, *Sep. Purif. Technol.*, 2016, **167**, 163–173.
11 M. Kárászová, J. Vejražka, V. Veselý, K. Friess, A. Randová, V. Hejtmánek, L. Brabec and P. Izák, *Sep. Purif. Technol.*, 2012, **89**, 212–216.
12 L. K. Chua, N. Jusoh and Y. F. Yeong, *Journal of Applied Science and Agriculture*, 2015, **10**, 215–221.
13 X. Y. Chen, H. Vinh-Thang, D. Rodrigue and S. Kaliaguine, *Ind. Eng. Chem. Res.*, 2012, **51**, 6895–6906.
14 M. Askari and T.-S. Chung, *J. Membr. Sci.*, 2013, **444**, 173–183.
15 V. Nafisi and M.-B. Hagg, *ACS Appl. Mater. Interfaces*, 2014, **6**, 15643–15652.
16 D. Sen, H. Kalipcilar and L. Yilmaz, *Desalination*, 2006, **200**, 222–224.
17 Y. Zhang, K. J. Balkus Jr, I. H. Musselman and J. P. Ferraris, *J. Membr. Sci.*, 2008, **325**, 28–39.
18 J. M. Duval, B. Folkers, M. H. V. Mulder, G. Desgrandchamps and C. A. Smolders, *J. Membr. Sci.*, 1993, **80**, 189–198.
19 A. A. S. Alomair, PhD dissertation, University of Manchester, 2013.
20 J. V. d. Bergh, W. Zhu, J. Gascon, J. A. Moulijn and F. Kapteijn, *J. Membr. Sci.*, 2008, **316**, 35–45.
21 D. Sen, PhD dissertation, Middle East Technical University, 2008.
22 A. E. Amooghin, *RSC Adv.*, 2015, **5**, 8552–8565.
23 M. U. M. Junaidi, C. P. Leo, A. L. Ahmad, S. N. M. Kamal and T. L. Chew, *Fuel Process. Technol.*, 2014, **118**, 125–132.
24 H. H. Yong, H. C. Park, Y. S. Kang, J. Won and W. N. Kim, *J. Membr. Sci.*, 2001, **188**, 151–163.
25 M. F. A. Wahab, A. F. Ismail and S. J. Shilton, *Journal of Chemical and Natural Resources Engineering*, 2008, **2**, 108–122.
26 O. Bakhtiari, S. Mosleh, T. Khosravi and T. Mohammadi, *J. Membr. Sci. Technol.*, 2011, **1**, 1–8.
27 F. R. Ribeiro, *Zeolites: Science and Technology*, Springer, Netherlands, 2012.
28 M. Qureshi and K. G. Varshney, *Inorganic Ion Exchangers in Chemical Analysis*, Taylor & Francis, 1991.
29 N. Y. Chen, T. F. Degnan and C. M. Smith, *Molecular Transport and Reaction in Zeolites: Design and Application of Shape Selective Catalysis*, John Wiley & Sons, 1994.
30 S. M. Mirfendereski, T. Mazaheri, M. Sadrzadeh and T. Mohammadi, *Sep. Purif. Technol.*, 2008, **61**, 317–323.
31 N. Azizi, T. Mohammadi and R. Mosayebi Behbahani, *Chem. Eng. Res. Des.*, 2017, **117**, 177–189.
32 F. Banihashemi, M. Pakizeh and A. Ahmadpour, *Sep. Purif. Technol.*, 2011, **79**, 293–302.
33 G. Clarizia, C. Algieri, A. Regina and E. Drioli, *Microporous Mesoporous Mater.*, 2008, **115**, 67–74.
34 S. L. Liu, R. Wang, Y. Liu, M. L. Chng and T. S. Chung, *Polymer*, 2001, **42**, 8847–8855.
35 V. Nafisi and M.-B. Hägg, *Sep. Purif. Technol.*, 2014, **128**, 31–38.
36 R. Wang, Y. Cao, R. Vora and R. J. Tucker, *J. Appl. Polym. Sci.*, 2001, **82**, 2166–2173.
37 S. N. Wijenayake, N. P. Panapitiya, S. H. Versteeg, C. N. Nguyen, S. Goel, K. J. Balkus, I. H. Musselman and J. P. Ferraris, *Ind. Eng. Chem. Res.*, 2013, **52**, 6991–7001.
38 Y. F. Yeong, H. Wang, K. Pallathadka Pramoda and T.-S. Chung, *J. Membr. Sci.*, 2012, **397–398**, 51–65.
39 N. Jusoh, K. K. Lau, A. M. Shariff and Y. F. Yeong, *Int. J. Greenhouse Gas Control*, 2014, **22**, 213–222.
40 M. Mubashir, Y. F. Yeong, K. Lau, T. Chew and N. Jusoh, *Sep. Purif. Technol.*, 2018, **199**, 140–151.
41 N. Jusoh, Y. F. Yeong, K. K. Lau and A. M. Shariff, *J. Cleaner Prod.*, 2017, **149**, 80–95.
42 D. Q. Vu, W. J. Koros and S. J. Miller, *Ind. Eng. Chem. Res.*, 2001, **41**, 367–380.
43 S. D. Kelman, *Crosslinking and Stabilization of High Fractional Free Volume Polymers for the Separation of Organic Vapors from Permanent Gases*, University of Texas at Austin, 2008.
44 S. Lock, K. Lau, A. Shariff, Y. Yeong, M. Bustam, N. Jusoh and F. Ahmad, *J. Nat. Gas Sci. Eng.*, 2018, **57**, 135–154.
45 N. Jusoh, Y. F. Yeong, M. Mohamad, K. K. Lau and A. M. Shariff, *Ultrason. Sonochem.*, 2017, **34**, 273–280.
46 M. D. Rad, S. Fatemi and S. M. Mirfendereski, *Chem. Eng. Res. Des.*, 2012, **90**, 1687–1695.
47 J. Jordens, T. Appermont, B. Gielen, T. Van Gerven and L. Braeken, *Cryst. Growth Des.*, 2016, **16**, 6167–6177.
48 J. A. Thompson, K. W. Chapman, W. J. Koros, C. W. Jones and S. Nair, *Microporous Mesoporous Mater.*, 2012, **158**, 292–299.
49 F. Franco, L. A. Pérez-Maqueda and J. L. Pérez-Rodríguez, *J. Colloid Interface Sci.*, 2004, **274**, 107–117.

50 D. Gandhi, Effect of Ostwald ripening on particle breakage in saturated solutions, *2007 AlChe Annual Meeting Proceedings*, San Francisco, 2007.
51 R. Zhou, L. Hu, Y. Zhang, N. Hu, X. Chen, X. Lin and H. Kita, *Microporous Mesoporous Mater.*, 2013, **174**, 81–89.
52 X. Chen, J. Wang, D. Yin, J. Yang, J. Lu, Y. Zhang and Z. Chen, *AIChE J.*, 2013, **59**, 936–947.
53 A. Mahmoudi, M. Namdari, V. Zargar, G. Khanbabaei and M. Asghari, *Int. J. Nano Dimens.*, 2014, **5**, 83–89.
54 W. Mozgawa, M. Krol and K. Barczyk, *Chemik*, 2011, **65**, 667–674.
55 S. Yang and N. P. Evmiridis, *Microporous Mater.*, 1996, **6**, 19–26.
56 X.-L. Zhang, L.-F. Qiu, M.-Z. Ding, N. Hu, F. Zhang, R.-F. Zhou, X.-S. Chen and H. Kita, *Ind. Eng. Chem. Res.*, 2013, **52**, 16364–16374.
57 L. Shao, T.-S. Chung, S. H. Goh and K. P. Pramoda, *J. Membr. Sci.*, 2004, **238**, 153–163.
58 W.-H. Lin, R. H. Vora and T.-S. Chung, *J. Polym. Sci., Part B: Polym. Phys.*, 2000, **38**, 2703–2713.
59 S. Basu, A. Cano-Odena and I. F. J. Vankelecom, *Sep. Purif. Technol.*, 2011, **81**, 31–40.
60 L. Shao, T.-S. Chung and K. P. Pramoda, *Microporous Mesoporous Mater.*, 2005, **84**, 59–68.
61 T. R. Crompton, in *Thermo-oxidative degradation of polymers*, Smithers Rapra, Akron, 2010, vol. 1, pp. 51–78.
62 Y. Li, T.-S. Chung, C. Cao and S. Kulprathipanja, *J. Membr. Sci.*, 2005, **260**, 45–55.
63 Y. Cui, H. Kita and K.-i. Okamoto, *J. Mater. Chem.*, 2004, **14**, 924–932.
64 Q. Jiang, J. Rentschler, G. Sethia, S. Weinman, R. Perrone and K. Liu, *Chem. Eng. J.*, 2013, **230**, 380–388.
65 S. Banerjee, *Handbook of Specialty Fluorinated Polymers: Preparation, Properties, and Applications*, Elsevier Science, 2015.
66 Y. P. Yampolskii, Y. Kamiya and A. Y. Alentiev, *J. Appl. Polym. Sci.*, 2000, **76**, 1691–1705.
67 T. T. Moore, R. Mahajan, D. Q. Vu and W. J. Koros, *AIChE J.*, 2004, **50**, 311–321.
68 T. Visser, N. Masetto and M. Wessling, *J. Membr. Sci.*, 2007, **306**, 16–28.
69 S. Velioğlu, M. G. Ahunbay and S. B. Tantekin-Ersolmaz, *J. Membr. Sci.*, 2012, **417–418**, 217–227.
70 A. Bos, I. G. M. Pünt, M. Wessling and H. Strathmann, *J. Polym. Sci., Part B: Polym. Phys.*, 1998, **36**, 1547–1556.
71 H. Eslami, M. Kesik, H. A. Karimi-Varzaneh and F. Müller-Plathe, *J. Chem. Phys.*, 2013, **139**, 124902.
72 X. Wang, Q. Su, J. Shan and J. Zheng, *Polym. Compos.*, 2016, **37**, 1705–1714.
73 S. Shahid and K. Nijmeijer, *J. Membr. Sci.*, 2014, **459**, 33–44.
74 A. M. W. Hillock, S. J. Miller and W. J. Koros, *J. Membr. Sci.*, 2008, **314**, 193–199.
75 M. Peydayesh, S. Asarehpour, T. Mohammadi and O. Bakhtiari, *Chem. Eng. Res. Des.*, 2013, **91**, 1335–1342.
76 Y. Li, T.-S. Chung, Z. Huang and S. Kulprathipanja, *J. Membr. Sci.*, 2006, **277**, 28–37.
77 T.-H. Bae, J. Liu, J. S. Lee, W. J. Koros, C. W. Jones and S. Nair, *J. Am. Chem. Soc.*, 2009, **131**, 14662–14663.

 